4th International Conference on Earthquake Engineering
Taipei, Taiwan
October 12-13, 2006

Paper No. 210

Debonding Monitoring of CFRP Strengthened RC Beams without Reference Data nor Prior Decision Boundaries

Hoon Sohn[1], Seung Dae Kim[2], Chi Won In[3], Kelly E. Cronin[4]and Kent Harries[5]

ABSTRACT

Fiber-reinforced polymer (FRP) composite materials have been widely used for retrofitting civil infrastructure systems. The ultimate goal of this study is to develop an in-site non-destructive testing (NDT) technique that can continuously and autonomously inspect the bonding condition between a carbon FRP (CFRP) layer and a host reinforced concrete (RC) structure, when the CRFP layer is used for strengthening the RC structure. The uniqueness of this reference-free NDT is two-fold: First, features, which are sensitive to CFRP debonding but insensitive to operational and environmental variations of the structure, have been extracted only from current data without direct comparison with previously obtained baseline data. Second, damage classification is performed instantaneously without relying on predetermined decision boundaries. The extraction of the reference-free features is accomplished based on the concept of time reversal acoustics, and the instantaneous decision making is achieved using cluster analysis. Monotonic and fatigue load tests of large-scale CFRP-strengthened RC beams are conducted to demonstrate the potential of the proposed reference-free debonding monitoring technique. Based on the experimental studies, it has been shown that the proposed reference-free NDT technique may minimize false alarms of debonding and unnecessary data interpretation by end users.

Keywords: cluster analysis, time-reversal acoustics, active sensing, baseline-free nondestructive testing, carbon fiber reinforced polymer, debonding, structural health monitoring.

INTRODUCTION

Fiber reinforced polymer (FRP) composite materials have become attractive alternate materials for retrofit and rehabilitation of civil infrastructure systems due to their outstanding strength, light weight and versatility (Karbhari et al. 2000). However, the improvement of strength and stiffness in a host structure can be guaranteed only when reliable bond between the host structure and the added FRP materials is maintained. Therefore, there is an increasing demand to inspect the initial installation quality and to monitor the long-term efficiency of bonded FRP retrofit measures. There is a large volume of research on damage detection techniques for FRP strengthened concrete structures. Acoustic emission (Mirmiran et al. 1999), infrared thermography (Levar and Hamilton 2003), fiber optic sensing (Ansari 2005), electromechanical impedance spectrum (Giurgiutiu et al. 2003), electrochemical impedance spectroscopy methods (Hong and Harichandran 2005), microwave sensing (Akuthota et al. 2004) and hybrid piezoelectric actuators/fiber optic sensors (Qing et al. 2006) have been applied. These techniques are shown to successfully identify FRP debonding. Although many damage detection techniques are successfully applied to scaled models or specimens tested in

[1] Assistant Professor, Carnegie Mellon Univ., Pittsburgh, PA 15213, Email: hsohn@cmu.edu
[2] Ph.D. Candidate, Carnegie Mellon Univ., Pittsburgh, PA 15213, Email: seungdak@andrew.cmu.edu
[3] Master Student, Carnegie Mellon Univ., Pittsburgh, PA 15213, Email: cin@andrew.cmu.edu
[4] Undergraduate Student, Carnegie Mellon Univ., Pittsburgh, PA 15213, Email: kcronin@andrew.cmu.edu
[5] Assistant Professor, Univ. of Pittsburgh, Pittsburgh, PA 15261, Email: kharries@engr.pitt.edu

controlled laboratory environments, the performance of these techniques in real operational environments is still questionable and needs to be validated. Varying environmental and operational conditions produce changes in the system's dynamic response that can be easily mistaken for damage (Sohn 2006). It is challenging to develop a NDT technique with minimal false positive and negative indications of damage when the system is exposed to varying environmental and operational conditions. Few NDT systems have been developed with the intent of deployment for continuous monitoring of in-service structures. In addition, data interpretation often needs to be manually performed by experienced engineers, and automation of data analysis remains largely unsolved. For continuous monitoring, it is critical to reduce unnecessary interference by users and to automate the data analysis process as much as possible.

The ultimate goal of this study is to develop a continuous NDT technique that can minimize false alarms of defects due to varying operational and environmental conditions expected in field applications and automatically diagnose the presence of damage based on a continuous stream of data. False indication of defects is reduced by extracting features sensitive to damage but insensitive to varying field conditions. Often, damage features are defined by comparing "current" data with "past" baseline data. However, these features are sensitive not only to the defect but also to other variations of the structure, making them vulnerable to false alarms. The dependency on these previously obtained baseline data is removed based on the concept of time reversal acoustics (TRA) in this study. Also, the decision making process for damage detection is often conducted by comparing the aforementioned damage features with a threshold value. The establishment of this decision boundary requires statistical modeling of the data obtained from intact conditions of the structure. This step needs human interaction, and the dependency of the training on the reference data again makes it susceptible to false alarms. To address this issue, damage classification is automated and conducted using cluster analysis (Seber, 1984). These concepts are introduced and the proposed NDT technique is applied to debonding detection during monotonic and fatigue tests of large-scale CFRP strengthened RC beams. Finally, the findings of this study are summarized and discussed.

EXTRACTION OF REFERENCE-FREE FEATURES BASED ON TIME REVERSAL ACOUSTICS

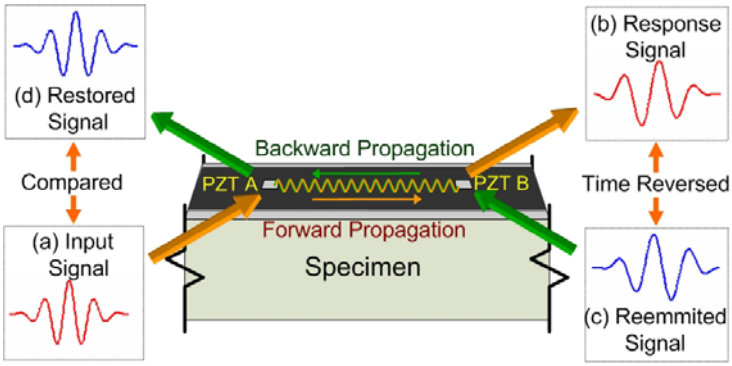

Figure 1. Schematic concept of TRA-based damage identification that does not require any pas baseline signals

The origin of the proposed time reversal process traces back to TRA (Fink and Prada 2001), and its concept is extended to guided wave propagations. In this extended time reversal process, a combination of a specific narrowband input waveform and multi-resolution signal processing is employed so that the time reversibility of guided waves is preserved within an acceptable tolerance for more complex configurations such as the layered structure presented in this study. Furthermore, surface mounted lead zirconate titanate (PZT) wafer transducers are used for generating and measuring guided waves (Giurgiutiu and Lyshevski 2004). According to the extended time reversal process shown in Figure 1, first a narrowband tone-burst signal is applied to PZT A. Then, elastic waves propagate through the medium and the response is measured at PZT B. Next, the strain time signal measured at PZT B is reversed in the time domain and applied back to PZT B after amplification.

Finally, the corresponding response is measured at PZT A; this response is called the "reconstructed" signal in this paper. According to TRA, the "shape" of the reconstructed signal should be identical to the original input signal after proper scaling. This time reversibility is based on the spatial reciprocity and time-reversal invariance of linear wave equations (Draeger et al. 1997).

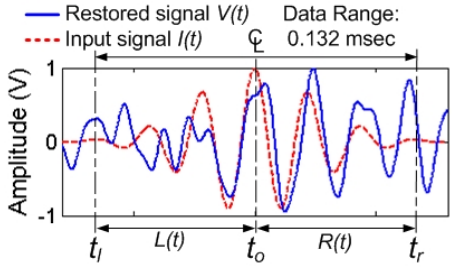

Figure 2. Definition of t_l, t_o, and t_r used in Equation (1) & (2)

The basic premise of TRA-based damage detection is that if there is a source of nonlinearity along the wave propagation path, the time reversibility and symmetry of the reconstructed signal break down. More precisely, the shape of the reconstructed signal's main peak will depart from that of the original input signal at the presence of nonlinear defects as shown in Figure 2. Because certain types of defects introduce nonlinear responses, examining the deviation of the reconstructed signal from the known initial input signal allows instantaneous identification of damage without requiring direct comparison with previously obtained baseline data. Based on this premise, two damage sensitive features are proposed for damage identification: time reversibility (TR) and symmetry (SYM) indices. The TR index, defined below, compares the waveform of the original input with that of the reconstructed signal:

$$\mathrm{TR} = 1 - \sqrt{\left\{\int_{t_l}^{t_r} I(t)V(t)\,dt\right\}^2 \Big/ \left\{\int_{t_l}^{t_r} I(t)^2\,dt \int_{t_l}^{t_r} V(t)^2\,dt\right\}} \qquad (1)$$

where *I(t)* and *V(t)* denote the known input signal and the main peak in the reconstructed signal, respectively. For the experimental study presented, a 7-peak toneburst signal is used for excitation; t_l and t_r represent the starting and ending time points of the signal as defined in Figure 2. The value of the TR index becomes zero when the shape of the main peak in the reconstructed signal is identical to that of the original input signal. Note that the amplitude scaling difference between *I(t)* and *V(t)* does not affect the TR value. If *V(t)* deviates from *I(t)*, the TR index value increases and approaches 1.0, indicating the existence of damage along the wave propagation path. The SYM index measures the degree of symmetry of the reconstructed signal with respect to the main peak in the middle.

$$\mathrm{SYM} = 1 - \sqrt{\left\{\int_{t_o}^{t_r} L(-t)R(t)dt\right\}^2 \Big/ \left\{\int_{t_l}^{t_o} L(t)^2\,dt \int_{t_o}^{t_r} R(t)^2\,dt\right\}} \qquad (2)$$

where *L(t)* and *R(t)* denote the left-hand and right-hand sides of the reconstructed signal with respect to the main peak, t_o is the center time point of the main peak and t_l and t_r represent the starting and ending time points as defined for the TR index. All terms are shown in Figure 2. The TR and SYM indices become inputs for the subsequent damage classification process.

BASELINE-FREE DAMAGE CLASSIFICATION USING CLUSTER ANALYSIS

Often decision making for damage detection is conducted by comparing some form of damage sensitive feature with a previously determined threshold value (Sohn et al. 2004). Once the feature value exceeds the decision boundary, the structure or the region where the feature is extracted is classified as damaged. Otherwise, it is concluded that the structure is in a pristine condition. This type of dichotomy classification requires the establishment of a threshold value based on statistical modeling of the features obtained from a known intact condition of the structure. Here, the drawback is that: (1) The estimation of the decision boundary necessitates collection of the baseline data and modeling of its statistical distribution, making this type of approach less attractive for autonomous

decision making and impractical (if not impossible) for existing structures, and (2) Since there can be a large time gap between when the decision boundary is established and damage actually occurs, the trustworthiness of the decision boundary becomes questionable for long-term continuous monitoring. To tackle these challenges, an instantaneous decision making process is developed in this section based on cluster analysis. The advantage of this cluster analysis is that it does not require statistical characterizations of baseline data for decision making. Previously, another type of reference-free damage classification was investigated based on sequential outlier analysis for detecting delamination in composite plates (Sohn et al. 2006). Sequential outlier analysis is more suitable when only a few outliers are expected while clustering analysis is better suited when equally populated data are expected from different classes.

Cluster analysis seeks to divide a set of data (damage sensitive features) into several classes so that data samples more similar to one another than they are to those in a different group can be grouped together. Cluster analysis is one particular case of unsupervised learning because the algorithm automatically classifies each sample based only on the distance measure provided. That is, the algorithm does not need any supervised learning with prior training data sets, and it is solely based on the current data set fed to the algorithm. Some of the algorithms commonly used for clustering include k-means, Gaussian mixture models, hierarchical clustering, self-organized mapping, subspace clustering, density-based algorithms, and graphic-based algorithms (Tan et al. 2005). In this study, the k-means cluster analysis is adopted for demonstration purposes. K-means clustering is an algorithm that classifies data sets into k number of groups based on their attributes or features (Gallant 1993). This grouping is performed by minimizing the Euclidian distance of each data point from the centroid of the corresponding group. Basically, the following three steps are iterated until no further change in clustering appears. Suppose there are four data points and each data point has two attributes/features as shown in Table 1. The objective of the k-means clustering is to group these data points into k=2 groups based on these features. For instance, it can be assumed that each data point has the TR and SYM indices as its features, and the goal is to assign them either to “undamaged” and “damaged” classes.

Table 1. An example data set for k-means clustering

	Sample A	Sample B	Sample C	Sample D
Feature 1	0.1	0.2	0.4	0.5
Feature 2	0.1	0.1	0.3	0.4

Step 1 - Estimation of class centroids: For a given number of k classes, the centroid of each class is arbitrarily assumed at the beginning. Often a subset of the available data points is designated as the centroids. Note that the final clustering is affected by this initial estimate of the centroids. Therefore, multiple iterations are repeated with different initial centroid positions. Suppose samples A and B are used as the initial centroids, and let C1 and C2 denote the coordinate of the centroids. Then, C1=[0.1, 0.1] and C2=[0.2, 0.1].

Step 2 - Estimation of distance measures: Next, the Euclidean distance from the cluster centroids to each sample point is computed as shown in Table 2.

Table 2. Euclidean distance of sample points from each cluster centroid

	Sample A	Sample B	Sample C	Sample D
Cluster 1	0.000	0.100	0.361	0.500
Cluster 2	0.100	0.000	0.283	0.424

Step 3 - Cluster Assignment: Each sample is assigned to a cluster based on the minimum distance. For instance, Sample A is assigned to Cluster 1, and the rest are assigned to Cluster 2 as shown in Table 3. The ultimate goal is to minimize the sum of sample-to-centroid distances over all clusters. This is achieved in two steps. In the first step, all samples are assigned to their nearest cluster centroid all at

once, and the cluster centroids are reevaluated for the next step. Then, more subtle tuning is performed by reassigning an individual sample to the other cluster. If this reassignment reduces the total sum of the distances, then the affected cluster centroid is recomputed after each reassignment. The new centroid for each cluster is assumed to be the average value of all sample data points assigned to the specific cluster. For instance, the new centroids for the next iteration become C1=[0.1, 0.1] and C2=[(0.2+0.4+0.5)/3, (0.1+0.3+0.44)/3] for the example presented in Table 3. The second step passes through all the samples for this reassignment. This iteration is repeated until its stability, meaning that switching of any additional sampling points does not minimize the sum of each cluster's Euclidean distances, is reached.

Table 3. Clustering of sampling points based on k-means algorithm

	Sample A	Sample B	Sample C	Sample D
Cluster 1	Assigned			
Cluster 2		Assigned	Assigned	Assigned

Although the existence of this convergence is proven (Anderberg, 1973), it does not guarantee the convergence to the global optimum point. That is, the final clustering result can be affected by the positions of the initially assumed centroids particularly when the number of samples is limited. Therefore, the selection of the initial starting centroids is critical to the success of cluster analysis. In this study, it is expected that the TR and SYM indices will be close to zero when there is no defect, and the index values will increase as debonding progresses. Based on this observation, the initial centroids for the undamaged and damaged classes are set to be 0.0 and 0.4, respectively. The main weakness of the k-means clustering is that the number of clusters must be known in advance. However, it may not be a serious problem in the present application because there are only two classes considered (undamaged and damaged).

DESCRIPTIONS OF EXPERIMENTS

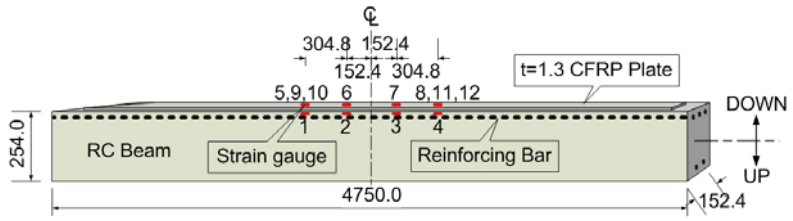

(a) Elevation of a CFRP strengthened RC beam with strain gauge locations (shown upside down)

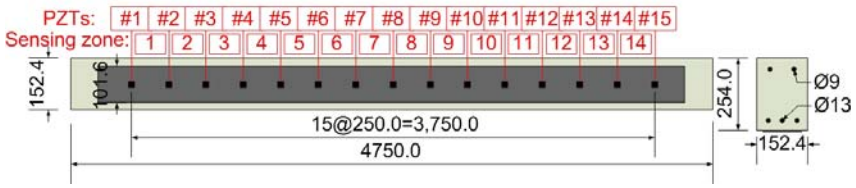

(b) An inverted plan view of the CFRP strengthened RC beam showing the PZT sensors and the sensing zones

Figure 3. Test setup and configuration of strain gauge and active sensing devices embedded/attached to the CFRP strengthened RC beam (all units are in mm)

The overall configuration of the test specimen is shown in Figure 3. The test specimen consists of a RC beam with a preformed CFRP strip. The RC beam is simply supported over 4750 mm as shown in Figure 3. It is reinforced with 3 #4 primary and 2 #3 compression reinforcing bars. The soffit-applied preformed CFRP strip is 102 mm wide and 1.3 mm thick. The CFRP strip has a manufacturer reported rupture strength and tensile modulus of 155 MPa and 2.8 MPa, respectively. This CFRP layer is applied over the middle 3750 mm of the beam span using an epoxy-based structural adhesive with a modulus of 2.2 MPa and a rupture strain of 0.006. Two such beam specimens were used in this study as described below. The load and strain data acquisition system includes (1) four electrical resistance

strain gauges (labeled as 1 to 4 in Figure 3(a)) attached to the internal reinforcing bars, (2) eight additional strain gauges mounted on the surface of the CFRP layer coincident with the previous strain gauges (labeled as 5 to 12 in Figure 3(a)), and (3) a load cell and a displacement transducer for measuring the applied load and displacement at the midspan of the beam. Note that Figure 3(a) shows the beam in an inverted position. These instruments were used to measure strains and to identify the presence of debonding at the discrete gauge locations. Details of the experimental setup and data analysis results based on strain measurements can be found in Harries et al. (2006). A total of 15 square PZT wafers (20 mm x 20 mm x 0.5 mm) were attached on the free surface of the CFRP layer at a uniform spacing of 250 mm along the beam to form a distributed active sensing system (Figure 3(b)). Because the PZTs produce an electrical charge when deformed, the PZT wafers were used as dynamic strain gauges The same PZT wafers are also used as actuators, because elastic waves are produced when an electrical field is applied to the wafers (Sun et al. 1995). In this experiment, excitation signals were applied to even number PZT wafers, and responses were measured at odd number PZTs. The time reversal process was repeated for a total of 14 sensing zones: #1 to #14 in Figure 3(b). The driving frequency value and the sampling rate were set to 45 kHz and 5 MHz, respectively.

Two loading cases were investigated in this study (Cases I and II). In Case I (Specimen L4 reported in Reeve 2005), the first specimen was subjected to incrementally increasing monotonic loading, and the data from the active sensing system were collected at each loading step. The monotonic load was gradually increased until the specimen failed. The loading was initially force-controlled up to loading step 5 (40.03kN) and then switched to displacement control as the beam "yielding" starting from loading step 6 (41.59 kN) to loading step 24 (44.54 kN). The second specimen (Specimen L4F reported in Zorn 2006) was subjected to fatigue loading. In Case II, cyclic loads with a driving frequency of 1.7Hz and an applied load range of 4.45 kN to 22.24 kN were applied. The specimen underwent a total of 2,000,000 fatigue load cycles over 16 days. Data from the active sensing system were gathered at 24 intermediate load cycles. During the data collection from the active sensing system, the cyclic load was paused at the minimum load of 4.45 kN. For both cases, there was an initial increase of the TR and SYM indices at the midspan point (sensing zone 7). It is speculated that the initial increases of the TR and SYM indices at sensing zone 7 did not result from debonding but rather from other unknown events. A 4.8 mm diameter steel rod was embedded in the concrete near sensing zone 7 for displacement measurement, and it may have affected the TR and SYM values. Therefore, these TR and SYM values at sensing zone 7 were disregarded and replaced with the average value of those from adjacent sensing zones 6 and 8.

EXPERIMENTAL RESULTS

The monotonic and fatigue load tests were performed on two CFRP strengthened RC beams to introduce debonding between the CFRP layers and the RC beams, and data were periodically collected from the active sensing system during the loading tests. The results of autonomous damage diagnosis based on the measured data a presented in this section for two loading cases (Cases I and II).

Case I: Monotonic Loading

The damage diagnosis obtained during the monotonic loading test of the first CFRP-RC beam specimen is presented in Figure 4. In Figure 4, the TR and SYM indices defined in Eqs. (1) and (2) are shown along the length of the beam and computed at selective loading steps. The sensing zones in Figure 4 are defined in Figure 3(b). It is observed from Figure 4 that: As loading increased, larger TR and SYM index values were observed near sensing zones 5 and 10. Overall, the findings from the proposed diagnosis system agreed well with visual inspection performed after the completion of the monotonic load test and the data obtained from the strain gauge system (Harries et al. 2006 and Reeve 2005).

Next, the TR and SYM indices values at sensing zones 10 and 14 are plotted as a function of the 24 loading steps in Figure 5. Figure 5 shows that the TR and SYM indices significantly increased at loading step 5 near sensing zone 10, but they did not vary much near sensing zone 14 throughout the

entire loading sequence. This finding is again in good agreement with the visual inspection performed after the completion of the monotonic loading test. In particular, it seems that the SYM index is more stable than the TR index when there is no debonding.

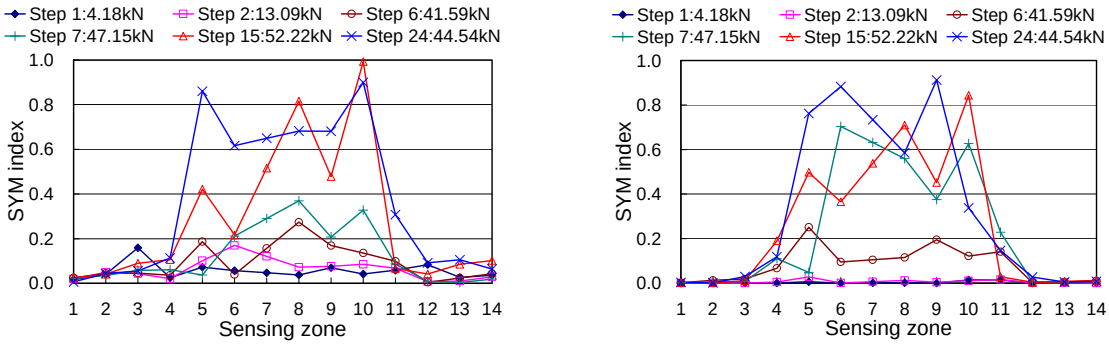

(a) TR indices at 6 selective loading steps (b) SYM indices at 6 selective loading steps

Figure 4. Changes of the TR and SYM indices measured at selective loading steps during the Case I monotonic loading test

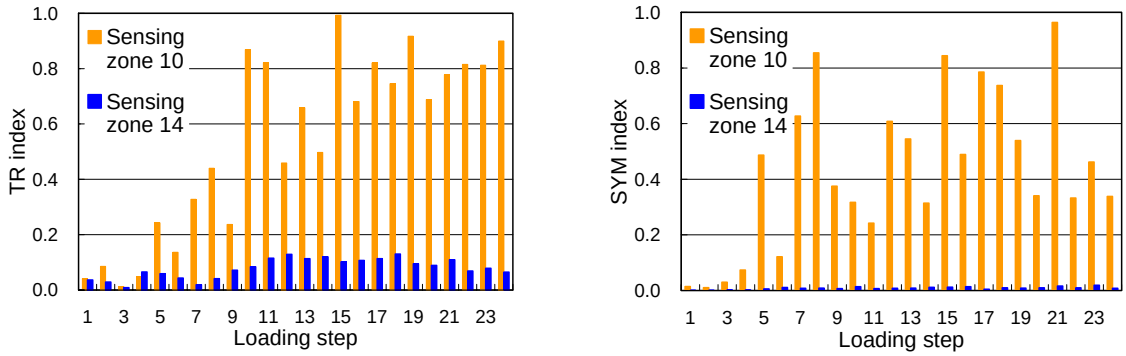

(a) TR indices at sensing zones 10 and 14 (b) SYM indices at sensing zones 10 and 14

Figure 5. Changes of TR and SYM indices as a function of incremental monotonic loading measured at sensing zones 10 and 14 for Case I

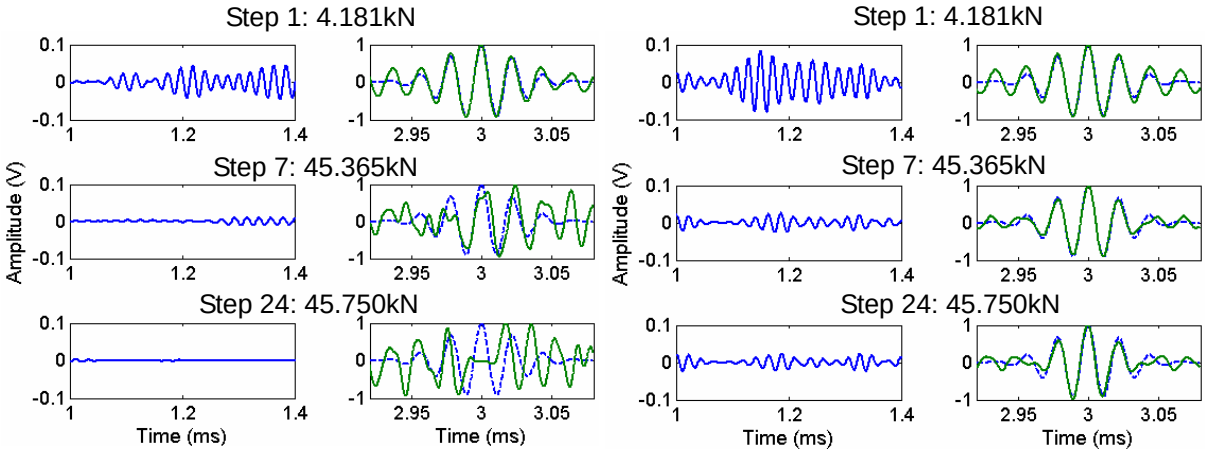

(a) Sensing zone 10 (b) Sensing zone 14

Figure 6. Forwarding and reconstructed signals measured at sensing zones 10 and 14 for Case I

The forwarding and reconstructed time response signals measured at sensing zones 10 and 14 are presented in Figure 6 for selective loading steps. The following observations are made from Figure 6: (1) As the load level increased, the static deflection of the beam increased near sensing zone 10. Consequently, the strain experienced by the bonded PZT material exceeded the maximum strain specified by the manufacturer (so-called “strain saturation”), and its response to the elastic waves

became less sensitive as shown in Figure 6(a); (2) Deviation of the reconstructed signal from the original input signal was observed at the increased load levels, indicating the initiation of debonding near sensing zone 10. To verify that the increases of the TR and SYM indices were not caused by the large strain deformation of the PZTs, a new set of PZT wafers were attached adjacent to the existing PZTs #5 through #11 following the completion of the monotonic load test (Kim et al., 2006). The data from the new PZT series was consistent with those from the old PZTs. Therefore, the changes of the TR and SYM indices are concluded to be related to debonding rather than PZT defects or strain saturation.

Qualitatively different results were obtained from sensing zone 14 located near one end of the beam. As mentioned previously, no sign of debonding was found near sensing zone 14. This is consistent with the finding that the reconstructed signal in Figure 6(b) did not change much throughout the entire loading history. However, it should be noted that the forwarding signal continuously changed as loading progressed. This observation clearly demonstrates the advantage of adopting the reconstructed signal for damage diagnosis rather than the conventional method of using only the forwarding signal: While the forwarding signal is sensitive to normal operational variations of the system that are not necessarily related to defects, the reconstructed signal seems to be more robust against these normal variations. Therefore, it is expected that the proposed debonding monitoring system based on the time reversal concept may be more suitable for field deployment and efficient for minimizing false-positive indications of defects.

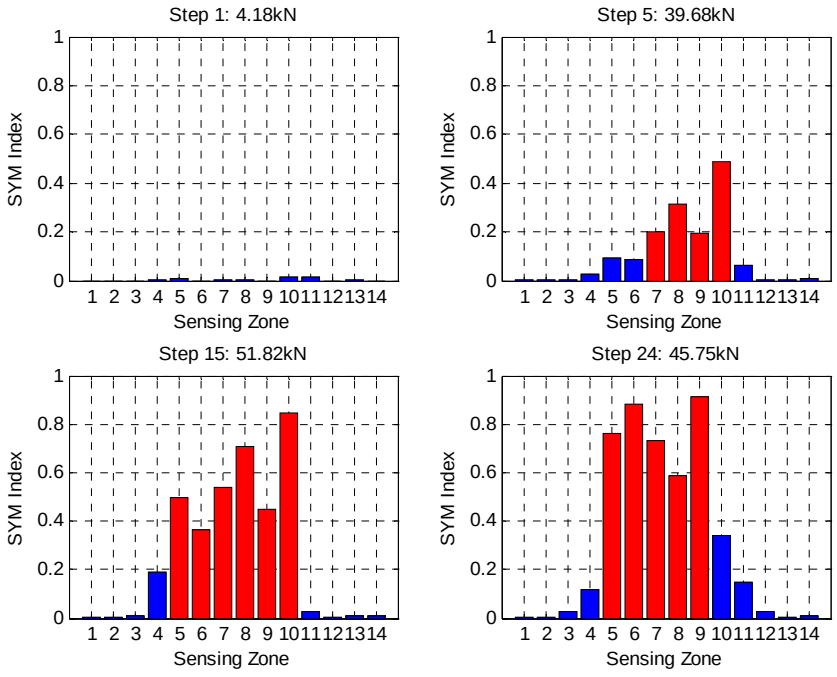

Figure 7. Autonomous damage classification using cluster analysis for Case I: Darker and lighter colors in the bar charts represent undamaged and damaged sensing zones, respectively

Next, the proposed cluster analysis is applied to the TR and SYM indices. The selective results obtained from cluster analysis of the SYM index are plotted in Figure 7. The darker and lighter colors in the bar charts represent the undamaged and damaged sensing zones, respectively. Up to loading step 3, there was no indication of debonding based on cluster analysis, and the first sign of debonding was shown in loading step 4. As the loading increased, the debonded zones spread out from the middle of the beam toward the beam edges. This progression of debonding is accurately detected by cluster analysis. Note that the diagnosis shown in Figure 7 is similar to an intuitive decision that a human observer might have drawn. When the SYM index values shown in Figure 7 are provided, one may instantly recognize that “something is wrong near the center of the beam” without having seen any prior baseline data. The proposed reference-free diagnosis attempts to imitate this human decision-making process.

Case II: Fatigue Cyclic Loading Test

The second specimen was subjected to 2,000,000 cycles of fatigue loading. In Figure 8, it was observed that the reconstructed signal did not change much although the forwarding signal varied significantly as the number of load cycles increased. Based on the cluster analysis, there was no sign of CFRP strip debonding from the substrate concrete beam during the fatigue loading test nor was any evidence of debonding found from visual inspection or a coin tapping test performed following the fatigue loading test. Additionally, no debonding was identified using the conventional strain gauge instrumentation (Zorn 2006).

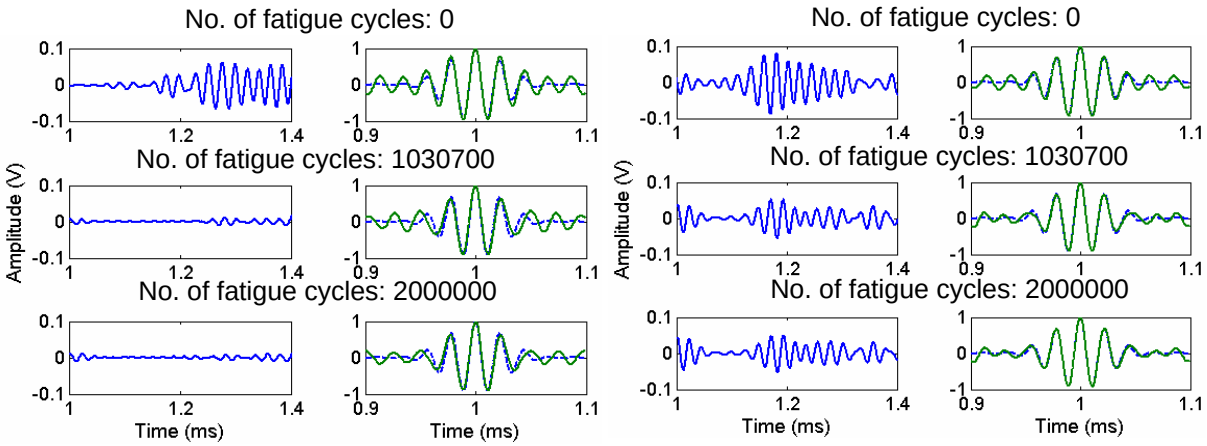

(a) Sensing zone 10 (b) Sensing zone 14

Figure 8. Forwarding and reconstructed signals measured at sensing zones 10 and 14 for Case II

CONCLUSION

A continuous monitoring system for detecting CFRP debonding from a host reinforced concrete structure is developed. The uniqueness of this study is in developing a new concept and theoretical framework of reference-free nondestructive testing (NDT), in which damage can be detected without direct comparison with previously obtained baseline data. Previously, a time reversal concept has been applied to extraction of damage-sensitive features that does not rely on direct comparison of current data with previously obtained baseline data. In this study, a statistical clustering technique is explored to develop a reference-free decision-making procedure so that the entire process of debonding monitoring can be automated without relying on prior decision boundaries or baseline signals for comparison.

The potential of the proposed reference-free approach was demonstrated using experimental data obtained from the loading tests of two CFRP strengthened RC beams: a monotonic load test (Case I), a fatigue load test (Case II). The proposed approach approximately estimated the initiation and region of debonding. The experimental results demonstrated the potential advantage of adopting the reference-free approach for damage diagnosis over conventional approaches: It is expected that the proposed reference-free NDT technique is more attractive for field deployment than conventional approaches because it is less sensitive to ambient variations of the structure. However, further research is necessary to eliminate false positive alarms of debonding.

ACKNOWLEDGEMENTS

This research was supported by Pennsylvania Infrastructure Technology Alliance (PITA) program. The authors would like to thank the PITA co-director, Prof. Cristina Amon for her support. The beam testing was assisted by Andrew Zorn and Benjamin Reeve in the Watkins-Haggart Structural Engineering Laboratory at the University of Pittsburgh.

REFERENCES

Akuthota, B., Hughes, D., Zoughi, R., Myers, J., and Nanni, A. (2004). "Near-Field Microwave Detection of Disbond in Carbon Fiber Reinforced Polymer Composites Used for Strengthening Cement-Based Structures and Disbond Repair Verification." *J. of Mater. in Civil Eng.*, 16(6), 540-546.

Anderberg, M.R. (1973). *Cluster Analysis for Applications*, Academic Press, New York.

Ansari, F. (2005). "Fiber optic health monitoring of civil structures using long gage and acoustic sensors." *Smart Mater. and Struct.*, 14(3), S1-S7.

Draeger, C., Cassereau, D., and Fink, M. (1997). "Theory of the time-reversal process in solids." *J. Acoust. Soc. Am.*, 102(3), 1289-1295.

Fink, M., and Prada, C. (2001). "Acoustic Time-Reversal Mirrors." *Inverse Problems*, 17, R1-R38.

Gallant, S. I. (1993). *Neural Network Learning and Expert Systems*, the MIT press, London, UK.

Giurgiutiu, V., and Lyshevski, S.E. (2004). *Micromechatronics: Modeling, analysis, and design with MATLAB*, CRC Press Inc, Boca Raton, FL.

Giurgiutiu, V., Harries, K.A., Petrou, M.F., Bost, J., and Quattlebaum, J. (2003). "Disbond Detection with Piezoelectric Wafer Active Sensors in RC Structures Strengthened with FRP Composite Overlays." *Earthquake Eng. and Eng. Vibration*, 2(2), 213-224.

Harries, K.A., Reeve, B. and Zorn, A. (2006). "Effect of Adhesive-line Properties on the Monotonic and Fatigue Behaviour of Externally Bonded CFRP Systems." *Proceedings of 11th International Conference on Structural Faults and Repair* Edinburgh, June 2006.

Hong, S., and Harichandran, R. (2005). "Sensors to Monitor CFRP/Concrete Bond in Beams Using Electrochemical Impedance Spectroscopy." *J. of Composite for Construction*, 9(6), 515-523.

Karbhari, V.M., Chin, J.W., and Reynaud, D. (2000). "Critical Gaps in Durability Data for FRP Composites in Civil Infrastructure." *Proc., 45th International Society for the Advancement of Materials and Process Engineering (SAMPE) Symposium and Exhibition*, Vol. 45, 549-563, Long Beach, CA, May 21-25.

Kim, S.D., In, C.W., Cronin, K.E., Sohn, H., Harries, K. (2006). "A Reference-Free NDT Technique for Debonding Detection in CFRP Strengthened RC Structures," *submitted to ASCE, Journal of Structural Engineering*.

Levar, J. and Hamilton, H. (2003). "Nondestructive Evaluation of Carbon Fiber-Reinforced Polymer-Concrete Bond Using Infrared Thermography." *ACI Mater. J.*, 100(1), 63-72.

Mirmiran, A., Shahawy, M., and Echary, H. (1999). "Acoustic Emission Monitoring of Hybrid FRP-Concrete Columns." *J. of Eng. Mech.*, 125(8), 899-905.

Qing, X.P., Wu, Z., Chang, F.K., Ghosh, K., Karbhari, V., Sikorsky, C. (2006). "Monitoring the Disbond of Externally Bonded CFRP Composite Strips for Rehabilitation of Bridges," *The Third European Workshop on Structural Health Monitoring*, Granada, Spain.

Reeve, B. (2005). "Effect of Adhesive Stiffness and CFRP Geometry on the Behavior of Externally Bonded CFRP Retrofit Measures Subject to Monotonic Loads." MS Thesis, University of Pittsburgh Department of Civil and Environmental Engineering.

Seber, G. A. F. (1984). Multivariate Observations, Wiley.

Sohn, H. (2006). "Effects of Environmental and Operational Variability on Structural Health Monitoring," *a Special Issue of Philosophical Transactions of the Royal Society on Structural Health Monitoring*, in press.

Sohn, H., Farrar, C.R., Hemez, F.M., Czarnecki, J.J., Shunk, D.D., Stinemates, D.W., Nadler, B.R. (2004). "A Review of Structural Health Monitoring Literature: 1996-2001," Los Alamos National Laboratory Report, LA-13976-MS.

Sohn, H., Park, H., Law, K., and Farrar, C. (2006). "Combination of a Time Reversal Process and a Consecutive Outlier Analysis for Baseline-free Damage Diagnosis," *J. of Intelligent Mater. Systems and Structures*, in press.

Tan, P.N., Steinback, M., Kumar, V. (2005)., *Introduction to Data Mining*, Addison-Wesley.

Zorn, A. (2006). "Effect of Adhesive Stiffness and CFRP Geometry on the Behavior of Externally Bonded CFRP Retrofit Measures Subject to Fatigue Loads." MS Thesis, University of Pittsburgh Department of Civil and Environmental Engineering.